J Mol Model (2012) 18:3553–3562
DOI 10.1007/s00894-012-1365-8

ORIGINAL PAPER

Equilibrium geometries, stabilities, and electronic properties of the cationic Au_nBe^+ (n=1-8) clusters: comparison with pure gold clusters

Peng Shao · Xiao-Yu Kuang · Ya-Ru Zhao · Yan-Fang Li · Su-Juan Wang

Received: 24 October 2011 / Accepted: 23 January 2012 / Published online: 14 February 2012

Abstract *Ab initio* method based on density functional theory at PW91PW91 level has been applied in studying the geometrical structures, relative stabilities, and electronic properties of small bimetallic Au_nBe^+ (n=1–8) cluster cations. The geometrical optimizations indicate that a transition point from preferentially planar (two-dimensional) to three-dimensional (3D) structures occurs at n=6. The relative stabilities of Au_nBe^+ clusters for the ground-state structures are analyzed based on the averaged binding energies, fragmentation energies, and second-order difference of energies. The calculated results reveal that the $AuBe^+$ and Au_5Be^+ clusters possess higher relative stability for small size Au_nBe^+ (n=1–8) clusters. The HOMO-LUMO energy gaps as a function of the cluster size exhibit a pronounced even-odd alternation phenomenon. Sequently, the natural population analysis and polarizability for our systems have been analyzed and compared further.

Keywords Au_nBe^+ cluster · Density functional method · Geometrical configuration

Introduction

Clusters containing atoms up to a few thousand represent an intermediate between single atom and bulk materials. Besides fundamental interest, extensive study of such species over the past decades has been motivated by their potential technological application in areas such as optics [1, 2], catalysis [3, 4], and photography [5]. Particularly, the impurity-doped clusters always exhibit more favorable and typical aspects of chemical activities than their host pure metals [6, 7]. Among the candidate systems that have been investigated, the doped gold bimetallic clusters attract more attention because of their particular physical and chemical properties and broad technological applications in almost all aspects of daily life [8–17].

In order to enhance the stability of gold clusters and improve their chemical activities, a great number of investigations on different impurity doped gold clusters have been performed [18–20]. For example, Yuan *et al.* [21] investigated the structures of Au_nM (n=1–7, M=Ni, Pd, Pt) clusters and found that the doped atoms can considerably alter the geometrical and electronic properties of the pure gold clusters. Zhang *et al.* [22] reported that $M@Au_6$ clusters (M=Sc–Ni), where the transition metal atoms are located in the center of Au_6 ring, could be used as a new nanomaterials with tunable magnetic moment. The structures and the electronic properties of $Au_{19}X$ clusters (X= Li, Na, K, Ru, Cs, Cu, and Ag) have been studied by Ghanty *et al.* [23]. As for doped gold cluster cations, the studies of cationic photofragmentation mass spectrometry (PMS) [24] on Au_nZn^+(n=2–44) clusters elucidated the anomalous stability of Au_5Zn^+. Theoretical studies of neutral and cationic Au_nZn clusters have been carried out by Tanaka *et al.*, who predicted that all of the lowest-energy isomers of Au_nZn ($n\leq6$) clusters and their cations are two dimensional (2D) structures similar to those of pure Au clusters [25]. Janssens *et al*. [26] using the cationic PMS investigated the stabilities of the $[Au_5X]^+$ (X=V, Mn, Cr, Fe, Co, Zn) clusters and the strongly enhanced abundance were found in them. Bouwen

P. Shao · X.-Y. Kuang (✉) · Y.-R. Zhao · Y.-F. Li · S.-J. Wang
Institute of Atomic and Molecular Physics, Sichuan University, Chengdu 610065, China
e-mail: scu_kuang@163.com

P. Shao
e-mail: shao19872005@126.com

X.-Y. Kuang
International Centre for Materials Physics, Academia Sinica, Shenyang 110016, China

et al. [27] and Heinebrodt *et al.* [28] studied the bimetallic $Au_nX_m^+$ clusters (X=Cu, Al, Y, In, Cs; n=1–65, m=1, 2).

Beryllium is a high melting, high boiling metal, with a rather high enthalpy of atomization. Beryllium-containing materials gained high importance in many key technologies including nuclear fission and nuclear fusion, radiation sources, high temperature ceramics for microelectronics, and high-performance alloys for naval, aircraft and space technology [29, 30]. Due to these unusual properties, theoreticians have extensively investigated beryllium clusters, and in particular, the dimer is a benchmark problem for quantum mechanical computations [31–33]. When one or two beryllium atoms are doped into neutral gold clusters, these corresponding isomers display an obvious even-odd alternation due to the closed opened-shell effects [34, 35]. Then we think about when one beryllium atom is doped into the cationic gold clusters, whether their structures and properties differ from those of the cationic bare gold clusters? And to the best of our knowledge, no systematical works for the bimetallic Au_nBe^+ clusters have been found. In this case, we have systematically reported a density functional theory investigation on the small size bimetallic Au_nBe^+ (n=1–8) clusters compared with those of the cationic pure gold clusters. In this paper, the geometrical structure, growth-pattern behaviors, relative stabilities, electronic properties, and polarizabilities of the small size Au_nBe^+ (n=1–8) clusters are investigated systematically. The geometrical optimizations indicate that a transition point from preferentially planar (two-dimensional) to three dimensional (3D) structures occurs at n=6. The calculated binding energy, fragmentation energy, second-order difference of energy, and the HOMO-LUMO gaps of Au_nBe^+ clusters show the same even-odd alternation tendency against cluster size. Furthermore, the natural electron configuration and polarizability have also been analyzed and compared further. It is hoped that our theoretical study not only would be useful for deeply understanding the influence of local structure on material's properties, but also can provide powerful guidelines for future experimental research.

Computational methods

Geometrical structure optimizations and frequency analysis of Au_nBe^+ (n=1–8) clusters have been performed by the density functional theory (DFT) method using the *GAUSSIAN 03* program [36] with the (Perdew/Wang 91) PW91PW91 [37] functional. The PW91PW91 model allows to obtain remarkable results both for covalent and noncovalent interactions in a quite satisfactory theoretical framework encompassing the free electron gas limit and most of the known scaling conditions. In present calculations, full electron calculation for the Au atom is rather time-consuming. Then, the basis set labeled GENECP are the combinations of LANL2TZ (f) [38] and 6–311+G (d) [39, 39] basis sets which are employed for the Au and Be atoms, respectively. As we all know, the relativistic effects play a primary role in the structure and energetic of Au-containing clusters. For Au, the relativistic effective core potentials (RECP) developed by Hay and Wadt [38] are chosen to represent the inner-core electrons, whereas the outer core orbitals (the 5*s* and 5*p*) are explicitly included in the Au valence shell. In this present work, our exchange-correlation functional is combined with the LANL2TZ (f) effective core potential and corresponding valence basis set. The reliability of current computational method has been tested by comparative calculations on AuBe and Au_2 molecules. The calculated bond length, and vibrational frequencies are presented in Table 1. It can be seen that the results based on PW91PW91 method are agree more with experimental values than others. This indicates the suitability of current computational method to describe the small size Au_nBe^+ (n=1–8) clusters.

In search of the lowest energy structure of cationic beryllium-doped gold clusters, the previous studies on positive gold clusters and neutral Au_nBe clusters are first employed as a guide [35, 42–44]. A great many of possible initial structures, which include one-, two- and three-dimensional configurations, have been considered in geometry optimizations and all the clusters are relaxed fully without any symmetry constraints. A large number of isomeric structures are obtained by placing/capping the Be atom on each possible site of the Au_n host clusters as well as substituting one Au by the Be atom from the Au_{n+1}. The larger sized cluster also can be obtained by placing one Au atom on $Au^+_{n-1}Be$ clusters. Due to the spin polarization, every initial structure is optimized at various possible spin multiplicities. It is worth pointing out that all of the clusters are found to prefer the lowest spin state. In order to confirm that the optimized geometry corresponds to a local minimum in potential energy, each of them is followed by an analysis of harmonic vibrational frequencies. By this way, a

Table 1 The calculated bond length (r) and frequency (ω_e) for the $AuBe^+$ and Au_2 clusters

	$AuBe^+$		Au_2	
Method	r (Å)	ω_e (cm^{-1})	r (Å)	ω_e (cm^{-1})
BP86	1.99	575.49	2.52	176.21
PW91P86	1.98	681.97	2.52	178.00
B3LYP	1.99	653.97	2.55	169.47
PW91PW91	**1.98**	**678.31**	**2.52**	**176.60**
Experimental	**1.98**[a]	**667.70**[a]	**2.47**[b]	**191.00**[b]

[a] Ref. [40] DK CASPT2 calculation

[b] Ref. [41]

large number of optimized isomers for Au_nBe^+ (n=1–8) clusters are obtained, but here we only list the few energetically low-lying isomers for each size in Fig. 1. In addition, the isomers of the ground-state Au_n^+ (n=2–9) cluster are also displayed in Fig. 1 for comparison. All charge populations were obtained with the natural population analysis (NPA) [45, 46], and the highest occupied-lowest unoccupied molecular orbital (HOMO-LUMO) gaps of the most stable isomers of Au_nBe^+ (n=1–8) were also obtained from PW91PW91 method with the identical basis set.

Results and discussion

Geometrical structures

A number of optimized low-lying isomers for Au_nBe^+ (n=1–8) clusters are shown in Fig. 1, and their corresponding relative energies, symmetries, and electronic state are summarized in Table 2. According to the energies from low to high, these isomers are designated by na, nb, nc, and nd, where n represents the number of Au atoms in the Au_nBe^+ clusters. Meanwhile, in order to examine the effects of dopant Be atom on gold clusters, geometry optimizations of Au_n^+ (n=2–9) clusters have been carried out using the identical method and basis set. The lowest-energy structures of Au_n^+ clusters are also displayed in Fig. 1.

According to the calculated results, the $AuBe^+$ isomer with $^1\sum$ state is manifested to be the lowest structure in all possible spin states, and the equilibrium bond length is 1.982 Å, which fits well with the results of Barysz [47] (1.982 Å) and Pyykkö [40] (1.983 Å). We calculated bond length of $AuBe^+$ using CCSD(T) method again, and the result is 198.4 pm which is agrees well with our previous calculation. Because $AuBe^+$ has a single bond, it should be compared with the single-bond covalent radii between Au and Be (226 pm) which was performed by Pyykkö [48, 49]. The curiouse difference may be because Pyykkö's covalent radii is the composition of ground-state electronic configuration, but $AuBe^+$ contains some excited states. Equilibrium bond distances of AuBe and $AuBe^-$ are also calculated using the identical method and basis set, and the calculated result are 2.053 Å and 2.170 Å respectively, which are both longer than that of cation (1.982 Å). The calculated results for the dissociation energies of AuBe and $AuBe^-$ dimer indicate that the Au-Be^- bond is stronger than the Au-Be and Au-Be^+ bonds.

All possible initial structures of Au_2Be^+ clusters, i.e., linear structures ($D_{\infty h}$, $C_{\infty v}$), and triangle structures (acute angle or obtuse angle) are optimized as the stable structures at PW91PW91 level with the different spin multiplicities. The linear 2a isomer with $D_{\infty h}$ symmetry is found to be the most stable isomer. The bond length of Au-Be is 2.07 Å and the corresponding electronic state is $^2\sum_u$. The 2b isomer with an obtuse angle is 1.30 eV higher in energy than the 2a isomer and it has C_s symmetry. When one Au atom of ground-state Au_3^+ cluster is replaced by Be atom, the trigonal 2c isomer in quartet spin state is obtained. In addition, the 2c isomer with the lowest spin state can not be found in our calculations.

Among the Au_3Be^+ clusters, both of the two distorted rhombus isomers 3a and 3c can be obtained by replacing different Au atoms in the most stable Au_4^+ cluster. They have the same C_{2v} symmetry and $^1A_1$ electronic state, while the former is 1.97 eV lower in energy than the latter. When one Be atom capped on the ground-state Au_3^+ structures, the Y-shaped isomer 3b emerges, in which the Be atom lies in the apex position. However, it is less stable than 3a isomer by 1.58 eV.

With regard to the Au_4Be^+ clusters, the most stable structure (4a) is a planar structure with $^2A_1$ state and C_{2v} symmetry. It can be obtained by adding one Au atom to the 3a structure. The W-shaped 4b isomer with incompact structure is energetically higher than the 4a isomer by 1.88 eV. When one Be atom is capped on the ground-state Au_4^+ structures, planar structure (4c) is generated. The average Au-Au bond length of 4c isomer is 2.709 Å, which is longer than that of the ground-state Au_4^+ cluster (2.686 Å). It hints that the capped Be atom makes the average Au-Au bond length of Au_4^+ cluster elongated. The planar isomer (4d) can be obtained by adding one Au atom to the 3b structure. From Table 2, one can see that the total energies of 4c and 4 d are 2.41 and 2.65 eV higher than that of 4a isomer, respectively.

In the case of Au_5Be^+ clusters, four isomers are shown in Fig. 1. Isomer (5a) with $^1A_1$ electronic state and C_{2v} symmetry is obtained by substituting the Be impurity for one Au atom in the ground-state Au_6^+ cluster. In order to reach the minimum of potential surface, the impurity atom has shifted along the gold atom original position. The 5b isomer, in which the Be atom is in the center and surrounded by five Au atoms, can be obtained by adding one Au atom to the 4a isomer. So it has high symmetry (D_{5h}). The 5c isomer, which can be viewed as the Be atom is capped on the side of the ground-state Au_5^+ cluster, has $^1A_1$ electronic state and C_{2v} symmetry. When one Au atom in the most stable Au_6^+ cluster is replaced by one Be atom, the planar 5 d isomer with $^1A_1$ electronic state can be obtained. Isomer 5b, 5c, and 5d are 0.12 eV, 1.40 eV, and 2.04 eV higher in energy than the 5a isomer respectively.

Starting at n=6, the lowest-energy structures of Au_nBe^+ clusters show appearance of 3D geometries. The 6a isomer, which has ^2A electronic state and C_s symmetry, is proved to be the most stable isomer for Au_6Be^+ clusters. Another 3D structure 6b isomer with C_s symmetry can be optimized as a stable structure, and it is less stable than 6a isomer by

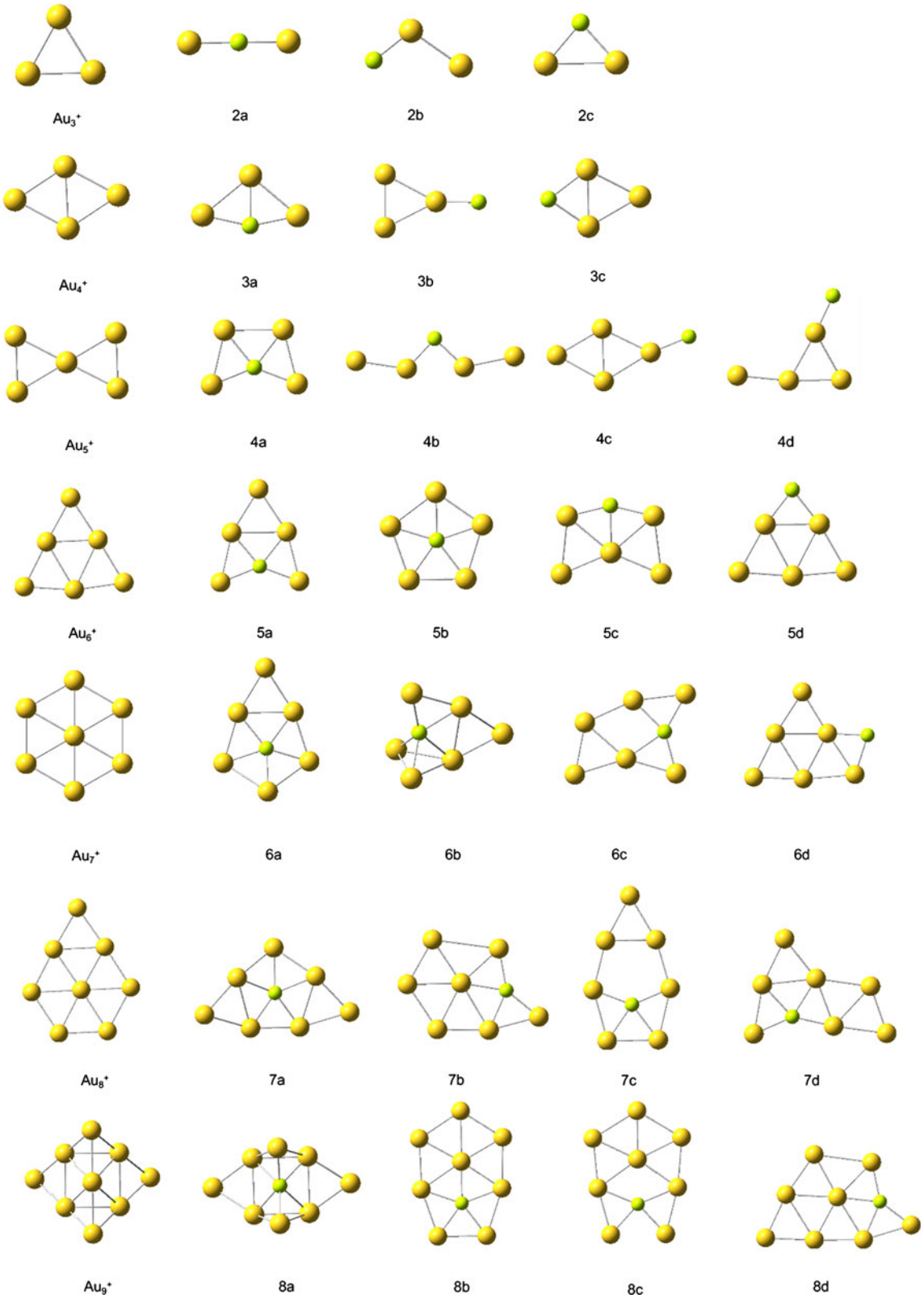

Fig. 1 The lowest energy structures of Au^{+}_{n+1} and Au_nBe^{+} (n=1–8) clusters, and some low-lying isomers for doped clusters. The yellow and green balls represent Au and Be atoms, respectively

Table 2 Geometries, symmetries, electron states, and relative energies ΔE (in eV) of Au_nBe^+ (n=1–8) clusters

	Sym	State	ΔE		Sym	State	ΔE
Au_2Be^+ (2a)	$D_{\infty h}$	$^2\sum_u$	0	Au_5Be^+ (5d)	C_{2v}	$^1A_1$	2.04
Au_2Be^+ (2b)	C_s	$^2A'$	1.30	Au_6Be^+ (6a)	C_s	^2A	0
Au_2Be^+ (2a)	C_{2v}	$^4B_2$	3.38	Au_6Be^+ (6b)	C_s	$^2A''$	0.18
Au_3Be^+ (3a)	C_{2v}	$^1A_1$	0	Au_6Be^+ (6c)	C_s	$^2A'$	0.24
Au_3Be^+ (3b)	C_{2v}	$^1A_1$	1.58	Au_6Be^+ (6d)	C_s	$^2A'$	1.76
Au_3Be^+ (3c)	C_{2v}	$^1A_1$	1.97	Au_7Be^+ (7a)	C_s	$^1A'$	0
Au_4Be^+ (4a)	C_{2v}	$^2A_1$	0	Au_7Be^+ (7b)	C_s	$^1A'$	0.34
Au_4Be^+ (4b)	C_{2v}	$^2A_1$	1.88	Au_7Be^+ (7c)	C_{2v}	$^1A_1$	0.60
Au_4Be^+ (4c)	C_s	$^2A'$	2.41	Au_7Be^+ (7d)	C_s	$^1A'$	0.77
Au_4Be^+ (4d)	C_s	$^2A'$	2.65	Au_8Be^+ (8a)	C_{2v}	$^2A_1$	0
Au_5Be^+ (5a)	C_{2v}	$^1A_1$	0	Au_8Be^+ (8b)	C_{2v}	$^2B_2$	0.11
Au_5Be^+ (5b)	D_{5h}	$^2A_1'$	0.12	Au_8Be^+ (8c)	C_{2v}	$^2A_1$	0.16
Au_5Be^+ (5c)	C_{2v}	$^1A_1$	1.40	Au_8Be^+ (8d)	C_s	$^2A'$	0.23

0.18 eV. Isomers 6c and 6d are proved to be two planar stable structures for Au_6Be^+ clusters, and both of them have the same $^2A'$ electronic state and C_s symmetry, but the former is 1.52 eV lower in total energy than the latter. The 6c isomer can be viewed as one Au atom cap on the 5a isomer, and when a Be atom is bi-capped on the ground-state Au_6^+ cluster, the stable structure (6d) is yielded.

As for Au_7Be^+ clusters, numerous possible initial geometries are optimized. According to the calculated results, the most stable isomer 7a, with C_s symmetry, can be viewed as one Au atom capping on the 6a isomer. It should be pointed out that this isomer (7a) is a 3D structure. If you take a good look at Fig. 1, you will find that both the isomer 7b and 7d can be viewed as two Au atoms bi-capping on the 5a isomer, and both of them have the same $^1A'$ electronic state and C_s symmetry. When one Be atom replaces the center Au atom of the ground-state Au_8^+ structures, the planar 7c isomer can be obtained. Isomer 7b, 7c, and 7d are 0.34 eV, 0.60 eV, and 0.77 eV higher in total energy than the 7a isomer respectively.

When the number of gold atoms is up to 8, we still find 3D isomer (8a) is the lowest energy structure, which has $^2A_1$ state and C_{2v} symmetry. It can be obtained by replacing the Au atom that lies in the central position by an impurity Be atom for the ground-state Au_9^+ cluster. Isomer 8b and 8c look like they have a similar structure, and they also have the same C_{2v} symmetry. However, their electronic state is different and the former is 0.05 eV lower in total energy than the latter. The planar 8d isomer can be viewed as one Au atoms bi-capping on the 7b isomer, and it has $^2A'$ state and C_s symmetry. Other planar and 3D isomers for the Au_8Be^+, which are not displayed in Fig. 1, are significantly higher in energy.

According to the above discussions, one can conclude that the ground-state structures of Au_nBe^+ (n=1–8) clusters favor the planar structures for n=2–5 and three-dimensional (3D) structure for n=6–8. Those results are quite different from the neutral Au_nBe clusters that we calculated before [35]. The Au-capped $Au^+_{n-1}Be$ clusters, Be-capped Au_n^+ clusters and Be-substituted Au_{n+1}^+ clusters are three kinds of dominating growth pattern for the Au_nBe^+ clusters. It is worth pointing out that all of the ground-state geometrical structure of Au_nBe^+ (n=1–8) clusters are not very similar to those of the cationic pure gold clusters but so much like those of the neutral Au_nBe clusters.

Relative stabilities

In order to investigate the relative stabilities of the most stable Au_nBe^+ (n=1–8) clusters, we have calculated the averaged binding energies $E_b(n)$, fragmentation energies $\Delta E(n)$ and second-order difference of energies $\Delta_2E(n)$. Considering the influence of impurity atom on the small pure clusters, all of the calculations above are compared with the pure Au^+_{n+1} clusters. For Au_nBe^+ clusters, $\Delta_b(n)$, $\Delta E(n)$, and $\Delta_2E(n)$ are defined as the following formula:

$$E_b(n) = [E(Be^+) + nE(Au) - E(Au_nBe^+)]/n + 1, \quad (1)$$

$$\Delta E(n) = E(Au_{n-1}Be^+) + E(Au) - E(Au_nBe^+), \quad (2)$$

$$\Delta_2E(n) = E(Au_{n-1}Be^+) + E(Au_{n+1}Be^+) - 2E(Au_nBe^+), \quad (3)$$

where $E(Au_{n-1}Be^+)$, $E(Au)$, $E(Be)$, $E(Au_nBe^+)$, and $E(Au_{n+1}Be^+)$ denote the total energies of the $Au_{n-1}Be^+$, Au, Be, Au_nBe^+ and $Au_{n+1}Be^+$ clusters, respectively.

For Au_n clusters, $E_b(n)$, $\Delta E(n)$, and $\Delta_2E(n)$ are defined as the following formula:

$$E_b(n+1) = [E(Au^+) + nE(Au) - E(Au^+_{n+1})]/n + 1, \quad (4)$$

$$\Delta E(n+1) = E(Au^{+}{}_{n}) + E(Au) - E(Au^{+}{}_{n+1}), \quad (5)$$

$$\Delta_2 E(n+1) = E(Au^{+}{}_{n}) + E(Au^{+}{}_{n+2}) - 2E(Au^{+}{}_{n+1}), \quad (6)$$

where $E(Au^{+}{}_{n+2})$, $E(Au)$, $E(Au^{+})$, $E(Au^{+}{}_{n})$, and $E(Au^{+}{}_{n+1})$ denote the total energies of the $Au^{+}{}_{n+2}$, Au, Au^{+}, $Au^{+}{}_{n}$, and $Au^{+}{}_{n+1}$ clusters, respectively.

The $E_b(n)$, $\Delta E(n)$, and $\Delta_2 E(n)$ values of the lowest energy $Au^{+}{}_{n+1}$ and Au_nBe^{+} (n=1–8) clusters against the

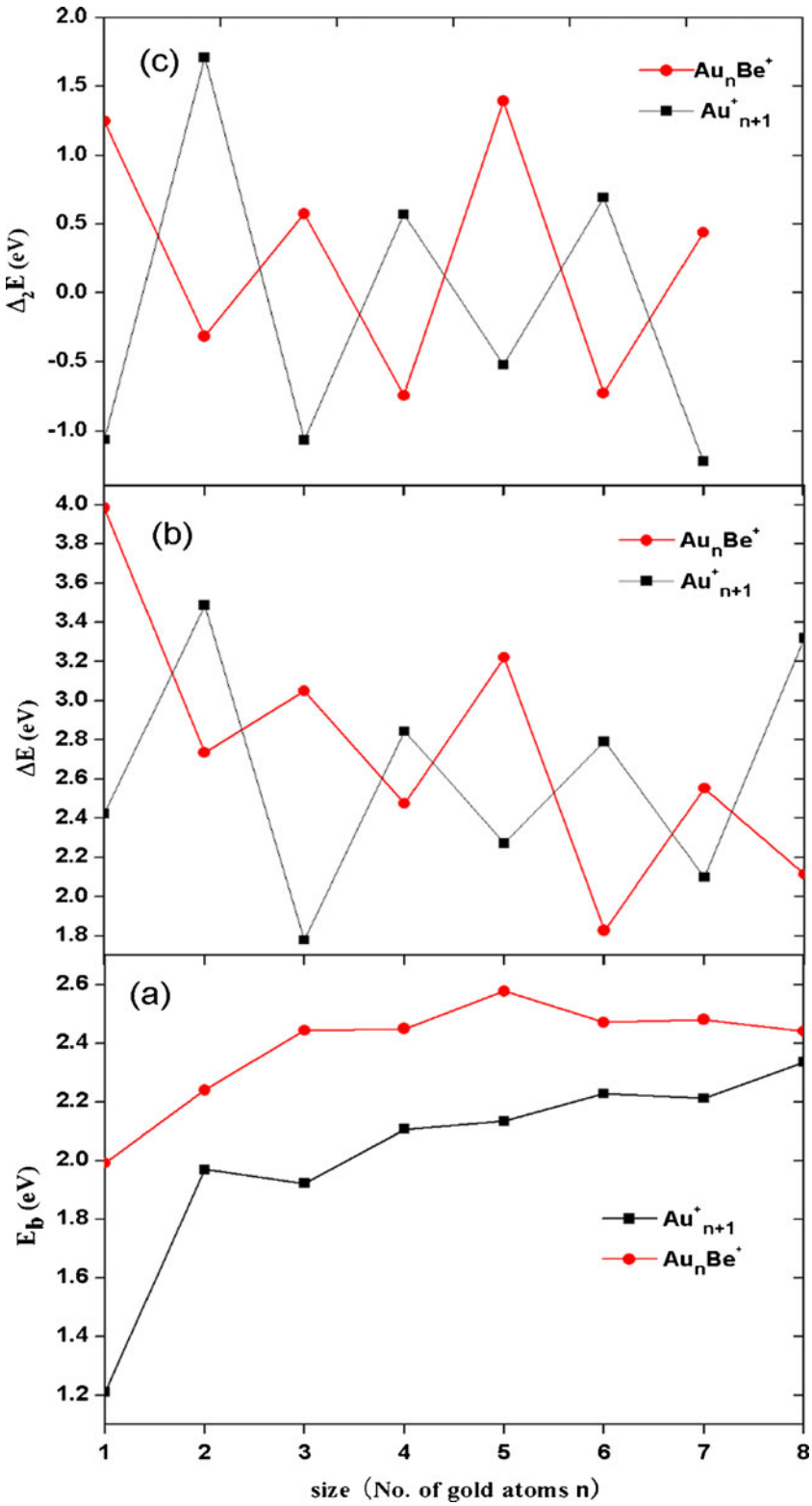

Fig. 2 Size dependence of the averaged binding energies $E_b(n)$(**a**), fragmentation energies $\Delta E(n)$ (**b**), and the second-order difference of energies $\Delta_2 E(n)$(**c**) for the lowest energy structures of $Au^{+}{}_{n+1}$ and Au_nBe^{+} (n=1–8) clusters

corresponding number of the Au atoms are plotted in Fig. 2. We can easily get the features of the size evolution and the peaks of the curves corresponding to those clusters having enhanced local stabilities. For Au^{+}_{n+1} clusters, the curves of the $E_b(n)$, $\Delta E(n)$, and $\Delta_2 E(n)$ values are all show an odd-even alternation phenomenon along with cluster size, where the clusters with odd numbers of Au atoms have higher values than the clusters with even numbers of Au atoms. This indicates a higher relative stability for the odd-sized clusters. A visible peak occurs at n=2. This hints that the Au_3^+ cluster is more stable than its neighboring clusters. For Au_3^+ the lowest-energy structure is an equilateral triangle (D_{3h}) (Fig. 1), which is also in good agreement with the BP86 functional CCSD(T) calculations [50] and ion mobility/DFT calculations made by Gilb *et al.* [44].

For Au_nBe^+ (n=1–8) clusters, the averaged binding energy is significantly higher than those of the corresponding sized Au^{+}_{n+1} clusters, reflecting that the stability of Au_nBe^+ is enhanced when Be is doped in the pure Au^{+}_{n+1} clusters. The curve increases smoothly when the size of Au_nBe^+ clusters increases from 1 to 5; then, it shows a slight even-odd alternation when n>5. Therefore, a visible peak occurs at n=5, indicating that Au_5Be^+ isomer is relatively more stable than its neighboring clusters. It is interesting to describe the enhanced stability for the Au_5Be^+ isomer due to a closed electron shell in a simple delocalized electron shell model. To examine the electron delocalization of Au_5Be^+, we have investigated the electronic structure and distribution of HOMOs. The Be atom forms extra σ bonding with the Au atoms through an overlap between vacant in-plane Be p obitals and valence Au s orbitals. This bonding interaction enhances the planarity of the cluster, because the *s-p* overlap is maximized when both Be and Au atoms are in the same plane. Another result of this in interaction is the stabilization of the HOMO of Au_5Be^+. The *s-p* overlap, which is responsible for the bonding character between Au and Be in the HOMO, has a stabilizing effect on the HOMO. The curve of the fragmentation energies and second-order difference of energies for Au_nBe^+ clusters almost have the same tendency. Both of them exhibit strong odd-even oscillations, indicating that odd-numbered gold doped clusters are relatively more stable than the neighboring even-numbered sized. Two conspicuous maxima are found at n=1 and 5. Accordingly, it can be indicated that $AuBe^+$and Au_5Be^+ clusters possess higher relatively stability and are magic clusters.

Electronic properties

We have examined the highest occupied-lowest unoccupied molecular orbital (HOMO-LUMO) energy gaps, which reflect the ability of electron to jump from occupied orbital to unoccupied orbital, and the results are shown in Fig. 3. The

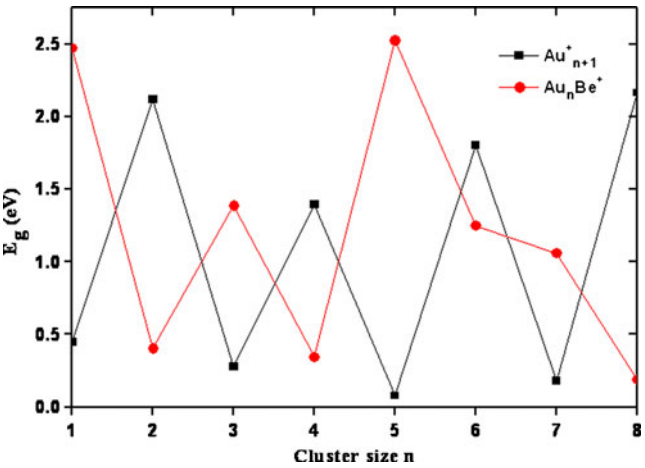

Fig. 3 Size dependence of the HOMO-LUMO energy gaps of ground-state Au^{+}_{n+1} and Au_nBe^+ (n=1–8) clusters

HOMO-LUMO energy gaps (E_g) rely on the eigenvalues of the HOMO and LUMO energy levels, and it is always considered to be a significant parameter that reflects chemical stability of small metal clusters. A large gap corresponds to a high strength required to perturb the electronic structure, namely a bigger gap indicates a weaker chemical activity. As shown in Fig. 3, the HOMO-LUMO energy gaps of Au_nBe^+ clusters also exhibit an odd-even oscillatory behavior when n≤5, namely, the clusters with odd number of atoms have an enhanced chemical stability due to their larger gaps compared with their neighbors. The electron pairing effect can explain the oscillatory trends. The odd-sized clusters have an even total number of valence electrons and the HOMO is doubly occupied. The electrons in a doubly occupied HOMO have stronger effective core potentials because the electron screening is weaker for electrons in the same orbital than for inner shell electrons. The clusters can more easily acquire an electron in the open-shell HOMO of the system with odd-numbered electrons than in the LUMO of a closed-shell system. That is in contrast to the Au^{+}_{n+1} clusters which have the opposite features.

Then the curve decrease sharply when the size of Au_nBe^+ clusters increases from 6 to 8. We can also find the magic clusters, $AuBe^+$ and Au_5Be^+ clusters, which have a particularly large energy gap. It means that $AuBe^+$ and Au_5Be^+ clusters possess dramatically enhanced chemical stability, which is in accord with the above analysis based on $E_b(n)$, $\Delta E(n)$, and $\Delta_2 E(n)$. Especially when n=5, there exit the largest energy gap difference (2.447 eV) between the Au_nBe^+ and Au_{n+1}^+ clusters, reflecting that the chemical stability of Au_5Be^+ is enhanced dramatically when Be atom is doped into the pure Au_5^+ clusters. Based on the above discussions, we can conclude that the $AuBe^+$ and Au_5Be^+ cluster can be seen as the building block of the novel material for its large relative stability and strong chemical stability.

Table 3 Natural charges populations of the lowest energy Au_nBe^+ (n=1–8) clusters

	Be	Au-1	Au-2	Au-3	Au-4	Au-5	Au-6	Au-7	Au-8
$AuBe^+$	0.886	0.114							
Au_2Be^+	0.402	0.299	0.299						
Au_3Be^+	0.254	0.179	0.179	0.388					
Au_4Be^+	−0.289	0.321	0.324	0.321	0.324				
Au_5Be^+	−0.102	0.300	0.115	0.271	0.300	0.115			
Au_6Be^+	−0.480	0.228	0.140	0.342	0.140	0.287	0.342		
Au_7Be^+	−0.293	0.195	0.141	0.332	0.144	0.144	0.141	0.195	
Au_8Be^+	−0.982	0.170	0.170	0.170	0.211	0.170	0.439	0.211	0.439

In order to probe into the localization of the positive charge in Au_nBe^+ clusters and investigate reliable charge-transfer information, the natural population analysis for the lowest energy Au_nBe^+ species have been calculated and the results are summarized in Table 3. From Table 3, it can be clearly seen that the beryllium atoms possess positive charges for n=1, 2, 3 and negative charges for n=4 to n=8. Those results quite agree with the neutral Au_nBe clusters that we calculated before [35]. While the gold atoms have positive charges all the time. It suggests that the charges in corresponding $Au_{4-8}Be^+$ clusters transfer from Au_n frame to the Be atom. Furthermore, we find an interesting relationship between the Be-Au bond length and the charges of Au atoms. In identical cluster, when two Au atoms have the same distance to the Be atom, they will have the same charges. This may suggest that the charge distribution is dependent on the symmetry of the cluster. Furthermore, in order to understand the electronic properties further, we have performed a detailed analysis of the onsite atomic charges of Be atom in Au_nBe^+ clusters. The charge of 2s, 2p, and 3s states for Be atoms in the most stable Au_nBe^+ clusters are shown in Table 4. It is shown that the 2s states have electrons 0.71–1.03, while the 2p states with 0.23–2.20 electrons. For the contribution from the 3s states, it is zero for n=1 to n=4, and starting at n=5, the 3s states begin to contribute 0.01 electrons.

Table 4 The charges of 2s, 2p, and 3s states for Be atoms in the most stable Au_nBe^+ systems

	Q (e)		
Cluster	Be-2s	Be-2p	Be-3s
Au_1Be^+	0.88	0.23	0
Au_2Be^+	1.03	0.55	0
Au_3Be^+	0.75	0.97	0
Au_4Be^+	0.84	1.42	0
Au_5Be^+	0.80	1.27	0.01
Au_6Be^+	0.73	1.71	0.01
Au_7Be^+	0.71	1.54	0.01
Au_8Be^+	0.72	2.20	0.01

Polarizability

It is well known that the static polarizability is a measure of the distortion of the electronic density and can provide the information about the response of the system under the effect of an external static electric field. It is very sensitive to the delocalization of the valence electrons and structures. As we all know, electron correlation effects are important for electric or magnetic properties. It is now well established that relativistic effective are important not only for inner atomic shells, but through relativistic direct, indirect and spin-orbital effects for valence shell as well [51]. Therefore, relativistic effective for polarizability cannot be neglected and has been included for our calculations. The average static polarizability is defined as: [52]

$$\langle a \rangle = \left(a_{xx} + a_{yy} + a_{zz}\right)/3. \quad (7)$$

In the current work, the polarizabilities for the lowest energy structures of Au_{n+1}^+ and Au_nBe^+ (n=1–8) clusters are shown in Fig. 4, and the plots of the beryllium-gold clusters polarizabilities along with the linear fit are shown as a function of n in the inserted figure of Fig. 4. As shown in

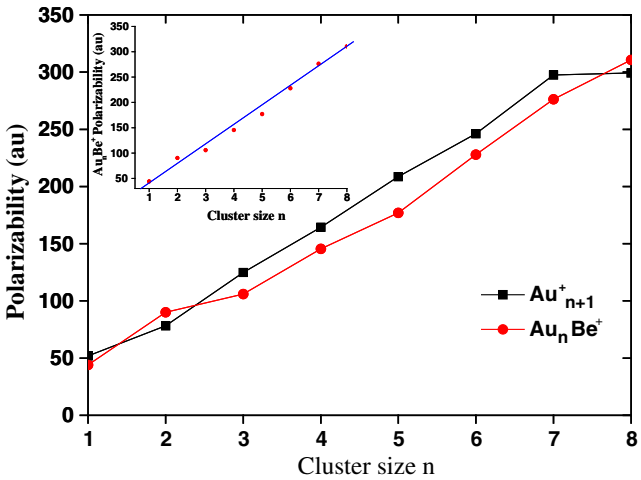

Fig. 4 Size dependence of the polarizabilities for the lowest energy structures of Au^+_{n+1} and Au_nBe^+ (n=1–8) clusters

the figure, we can find that the polarizabilities of cationic gold cluster increase as a function of cluster size n, modulated by these linearity, up to n=8. Thus, in the Au_{n+1}^+ clusters the electrons are more strongly attracted by the nuclei and their electronic structure is more compact. The minimum polarizability principle (MPP) states that any system evolves naturally toward a state of minimum polarizability [53, 54]. By applying the MPP to chemical reactivity, those clusters with the local minimum polarizability are more stable than the neighboring clusters. Two obvious minimum occur at n=2 and 8, indicating that the Au_3^+ and Au_9^+ cluster have enhanced electric stability, which is in accord with the above analysis.

For the Au and Be atoms, our calculated values were 34.0 and 42.9 a.u., respectively. Our results are in reasonable agreement with the reported experimental estimate of 39.1±9.8 a.u. [55] for Au atoms and the theoretical value of 45.09 a.u. [56] for Be atoms. The value for the Au atom was smaller than that for the Be atom, which was due to the enhanced screening of the s electrons by the d electrons in Au atoms. The values of $\langle a \rangle$ for Au_nBe^+ clusters almost display the same trend with cationic gold cluster. Overall, $\langle a \rangle$ increases as a function of n, modulated by these oscillations, up to n=8. It is almost along with the liner variation y=38.087x. Otherwise, the curve of $\langle a \rangle$ displays an obvious minimum occurs at n=5, which indicates that Au_5Be^+ isomer has dramatically enhanced electric stability than its neighboring clusters. This result is also in accord with the above analysis.

Conclusions

The geometrical structure, growth-pattern behaviors, relative stabilities, electronic properties, and polarizabilities of the small size Au_nBe^+ (n=1–8) clusters have been investigated systematically by density functional theory at the PW91PW91/GENECP level. All the results are summarized as follows.

(i) The geometrical optimizations indicate that the ground-state structures of Au_nBe^+ (n=1–8) clusters favor the planar structures for n=2–5 and three-dimensional (3D) structure for n=6–8. Au-capped $Au^+_{n-1}Be$ clusters, Be-capped Au^+_n clusters and Be-substituted Au^+_{n+1} clusters are three kinds of dominating growth pattern for the Au_nBe^+ clusters.

(ii) The calculated binding energies, fragmentation energies, second-order difference of energies, and the HOMO-LUMO gaps of Au_nBe^+ clusters show the same odd-even alternation tendency with cluster size. It indicates that Au_nBe^+ clusters with odd-numbered n are relatively more stable than the neighboring even-numbered sized. $AuBe^+$ and Au_5Be^+ clusters are tested to possess higher relatively stability and enhanced chemical stability.

(iii) Our natural population analysis (NPA) results show that in identical cluster, if two Au atoms have the same Au-Be bond, they will have the same local charges. Moreover, polarizabilities of Au_nBe^+ clusters depend sensitively on the cluster size and an obvious minimum occurs at n=5.

Acknowledgments The authors are grateful to the National Natural Science Foundation of China (Nos. 10974138)

References

1. Logunov SL, Ahmadi TS, El-Sayed MA, Khoury JT, Whetten RLJ (1997) Phys Chem B 101:3713–3719
2. Gaudry M, Lerme J, Cottancin E, Pellarin M, Vialle JL, Broyer M, Prevel B, Treilleux M, Melinon P (2001) Phys Rev B 64:085407
3. Sanchez A, Abbet S, Heiz U, Schneider WD, Haekkinen H, Barnett RN, Landman U (1999) J Phys Chem A 103:9573–9578
4. Schnabel P, Irion MP, Weil KG (1991) J Phys Chem 95:9688–9694
5. Fayet P, Granzer F, Hegenbart G, Moisar E, Pischel B, Woeste L (1985) Phys Rev Lett 55:3002–3004
6. Zehner DM, Goodman DM (1987) Mater Res Soc 83:59–64
7. Rodriguez JA (1996) Surf Sci Rep 24:223–287
8. Majumder C, Kandalam AK, Jena P (2006) Phys Rev B 74:205437
9. Li X, Kiran B, Cui LF, Wang LS (2005) Phys Rev Lett 95:253401
10. Graciani J, Oviedo J, Sanz JF (2006) J Phys Chem B 110:11600–11603
11. Teles JH, Brode S, Chabanas M (1998) Angew Chem 99:2589–2593
12. McRae R, Lai B, Vogt S, Fahrni CJ (2006) J Struct Biol 155:22–29
13. Ackerson CJ, Jadzinsky PD, Jensen GJ, Kornberg RD (2006) J Am Chem Soc 128:2635–2640
14. Xiao L, Wang L (2004) Chem Phys Lett 392:452–455
15. Die D, Kuang XY, Gou JJ, Zheng XB (2010) J Phys Chem Solids 71:770–776
16. Bürgel C, Reilly NM, Johnson GE, Mitrić R, Kimble ML, Castleman AW Jr, Bonačić-Koutecký V (2008) J Am Chem Soc 130:1694–1698
17. Zhai HJ, Li J, Wang LS (2004) J Chem Phys 121:8369–8374
18. Koszinowski K, Schröder D, Schwarz H (2003) Chem Phys Chem 4:1233–1237
19. Häkkinen H, Abbet S, Sanchez A, Heiz U, Landman U (2003) Angew Chem Int Ed 42:1297–1300
20. Pyykkö P, Runeberg N (2002) Angew Chem Int Ed 41:2174–2176
21. Yuan DW, Wang Y, Zeng Z (2005) J Chem Phys 122:114310
22. Zhang M, He LM, Zhao LX, Feng XJ, Luo YH (2009) J Phys Chem C 113:6491–6496
23. Ghanty TK, Banerjee A, Chakrabarti A (2010) J Phys Chem C 114:20–27
24. Tanaka H, Neukermans S, Janssens E, Silverans RE, Lievens P (2003) J Am Chem Soc 125:2862–2863
25. Tanaka H, Neukermans S, Janssens E, Silverans RE, Lievens P (2003) J Chem Phys 119:7115–7124
26. Janssens E, Tanaka H, Neukermans S, Silverans RE, Lievens P (2003) New J Phys 5(46):1–46.10
27. Bouwen W, Vanhoutte F, Despa F, Bouckaert S, Neukermans S, Kuhn LT, Weidele H, Lievens P, Silverans RE (1999) Chem Phys Lett 314:227–233

28. Heinebrodt M, Malinowski N, Tast F, Branz W, Billas IML, Martin TP (1999) J Chem Phys 110:9915–9922
29. Petzow G, Zorn H (1974) Chem Ztg 98:236–241
30. Takagi T, Matsubara K, Takaoka H (1980) J Appl Phys 51:5419–5424
31. Starck J, Meyer W (1996) Chem Phys Lett 258:421–426
32. Martin JML (1999) Chem Phys Lett 303:399–407
33. Gdanitz RJ (1999) Chem Phys Lett 312:578–584
34. Zhao YR, Kuang XY, Zheng BB, Wang SJ, Li YF (2010) J Mol Modeld doi:10.1007/s00894-011-1051-2
35. Chen DD, Kuang XY, Zhao YR, Shao P, Li YF (2010) Chin Phys B 20:063601
36. Frisch MJ, Trucks GW, Schlegel HB, Scuseria GE, Robb MA, Cheeseman JR, Montgomery JAJr, Vreven T, Kudin KN, Burant JC, Millam JM, Iyengar SS, Tomasi J, Barone V, Mennucci B, Cossi M, Scalmani G, Rega N, Petersson GA, Nakatsuji H, Hada M, Ehara M, Toyota K, Fukuda R, Hasegawa J, Ishida M, Nakajima T, Honda Y, Kitao O, Nakai H, Klene M, Li X, Knox JE, Hratchian H P, Cross JB, Bakken V, Adamo C, Jaramillo J, Gomperts R, Stratmann RE, Yazyev O, Austin AJ, Cammi R, Pomelli C, Ochterski JW, Ayala PY, Morokuma K, Voth GA, Salvador P, Dannenberg JJ, Zakrzewski VG, Dapprich S, Daniels AD, Strain MC, Farkas O, Malick DK, Rabuck AD, Raghavachari K, Foresman JB, Ortiz JV, Cui Q, Baboul AG, Clifford S, Cioslowski J, Stefanov B, Liu G, Liashenko A, Piskorz P, Komaromi I, Martin RL, Fox DJ, Keith T, Al-Laham MA, Peng CY, Nanayakkara A, Challacombe M, Gill PMW, Johnson B, Chen W, Wong MW, Gonzalez C, Pople JA (2004) Gaussian 03, Revision E.01. Gaussian, Wallingford, CT
37. Perdew P, Chevary JA, Vosko SH, Jackson KA, Pederson MR, Singh DJ, Fiolhais C (1992) Phys Rev B 46:6671–6687
38. Hay PJ, Wadt WR (1985) J Chem Phys 82:299–310
39. Krishnan R, Binkley JS, Seeger R, Pople JA (1980) J Chem Phys 72:650–655
40. Hehre WJ, Radom L, Schleyer PVR, Pople JA (1986) *Ab initio* molecular Orbital Theory. Wiley, New York
41. Barysz M, Pyykkö P (1998) Chem Phys Lett 285:398–403
42. Ajanta D, Ramesh CD (2008) J Mol Struct THEOCHEM 870:83–93
43. Torres MB, Fernández EM, Balbás LC (2005) Phys Rev B 71:155412
44. Nagy G, Gelb LD, Walker AV (2005) J Am Soc Mass Spectrom 16:733–742
45. Gilb S, Weis P, Furche F, Ahlrichs R, Kappes MM (2002) J Chem Phys 116:4094–4102
46. Reed AE, Weinstock B, Weinhold F (1985) J Chem Phys 83:735–747
47. Reed AE, Curtiss LA, Weinhold F (1988) Chem Rev 88:899–926
48. Balducci G, Ciccioli A, Gigli G (2004) J Chem Phys 112:7748–7755
49. Pyykkö P, Atsumi M (2009) Chem Eur J 15:12770–12779
50. Pyykkö P (2005) Inorg Chim Acta 358:4113–4130
51. Wesendrup R, Hunt T, Schwerdtfeger P (2000) J Chem Phys 112:9356–9362
52. Pyykkö P (1988) Chem Rev 88:563–594
53. Gupta K, Ghanty TK, Ghosh SK (2010) Phys Chem Chem Phys 12:2929–2934
54. Chattaraj PK, Sengupta S (1996) J Phys Chem 100:16126–16130
55. Chattaraj PK, Fuentealba P, Jaque P, Toro-Labbé A (1999) J Phys Chem A 103:9307–9302
56. Roos BO, Liudh R, Malmqvist PA, Veryazov V, Widmark PO (2005) J Phys Chem A 109:6575–6579
57. Bégué D, Mérawa M, Rérat M, Pouchan C (1999) Chem Phys Lett 301:43–52